Journal of Molecular Liquids 398 (2024) 124215

Contents lists available at ScienceDirect

Journal of Molecular Liquids

journal homepage: www.elsevier.com/locate/molliq

Preparation and characterization of biodegradable gelatine and starch films embedding cerium oxide nanoparticles stabilized by PLGA micelles for antibiofilm applications

Verdiana Marchianò [a,b], Maria Matos [a,c], Ismael Marcet [a], M. Carmen Blanco-López [b,c], Gemma Gutiérrez [a,c,*], Nicola Cioffi [d], Nicoletta Ditaranto [d,*]

[a] Department of Chemical and Environmental Engineering, University of Oviedo, Oviedo, Spain
[b] Department of Physical and Analytical Chemistry, University of Oviedo, Oviedo, Spain
[c] Instituto Universitario de Biotecnología de Asturias, University of Oviedo, Oviedo, Spain
[d] Dipartimento di Chimica and CSGI—Bari Unit, Università degli Studi di Bari Aldo Moro, Bari, Italy

ARTICLE INFO

Keywords:
Cerium oxide nanoparticles
Biodegradable films
Antibiofilm activity
Food packaging
PLGA micelles
X-ray photoelectron spectroscopy

ABSTRACT

Cerium oxide nanoparticles (CeO_2NPs) have been widely investigated for numerous applications due to their redox activity, free radical scavenging property, and biofilm inhibition. Here we describe a new antibiofilm system based on CeO_2NPs protected and stabilised by PLGA micelles embedded in two different biodegradable and biocompatible films. CeO_2NPs were synthesised following the W/O microemulsion method and subsequently encapsulated in PLGA micelles according to the single emulsion/solvent procedure. All formulations (free NPs, empty micelles and loaded micelles) were incorporated in gelatine and starch films aimed at food packaging use. The chemical and physical characterizations of the NPs and micelles solutions were carried out by Dynamic Light Scattering (DLS), Transmission Electron Microscopy (TEM) and X-ray Photoelectron Spectroscopy (XPS). Blank films and films incorporating micelles and NPs were also characterized by Scanning Electron Microscopy (SEM) and by XPS. Antibacterial experiments were also performed to investigate the system viability for the final use.

1. Introduction

Bacterial infections are among the most severe diseases affecting human beings and have become challenging to eliminate due to antibiotic resistance. Nanotechnology offers a potential solution through the use of drug delivery therapy to treat infectious diseases. Over the years, metal and metal oxide nanoparticles have attracted the attention of many researchers for their use in a wide range of biomedical applications for their unique physical and chemical properties [1–17].

Among the others, CeO_2 nanoparticles synthesized using various methods have been extensively studied [18]. Cerium is one of the rare earth elements that have shown promising antimicrobial activity. CeO_2 has a cubic structure, which contributes to its optical and electronic properties, and it is the only lanthanide stable in tetravalent state, that is the active valence state for antimicrobial purposes. In the biomedical field, CeO_2 is utilized for its capacity to scavenge reactive oxygen species (ROS) and its distinctive antibacterial properties against both Gram-positive and Gram-negative bacteria as well as fungi [19–21]. The CeO_2NPs are used for topic treatments [22], incorporated in hydrogel formulations [23], for tissue engineering scaffolds [24], because they stimulate the proliferation of cells in vitro [24,25], gene therapy, and improves implants' biodegradability [26]. Their antimicrobial mechanism is probably related to the oxidative stress of microorganism cell membrane components. It is thought in general that the main mechanism is based on the adsorption of CeO_2NPs through the bacterium membrane. This is facilitated by the acidic pH at the site of infection, since at a low pH the NPs become positively charged and more easily adhere to the negatively charged bacteria through electrostatic interactions. During this process, the surface of CeO_2NPs undergoes chemical reduction, converting Ce^{4+} to Ce^{3+} [27].

Thil et al. [28] suggested three types of interaction between bacteria and CeO_2NPs: (1) adsorption, (2) oxi-reduction, and (3) toxicity. In other hand, the interaction with fungi, for examples Candida albicans [29], probably is due to an interaction with a component of fungal cell wall causing an irreversible change such as blocking fungal enzymatic activity.

* Corresponding authors.
E-mail addresses: gutierrezgemma@uniovi.es (G. Gutiérrez), nicoletta.ditaranto@uniba.it (N. Ditaranto).

https://doi.org/10.1016/j.molliq.2024.124215
Received 29 August 2023; Received in revised form 28 December 2023; Accepted 4 February 2024
Available online 7 February 2024

The main disadvantage of free CeO_2NPs is that they can be easily excreted from the organism or can be dissolved to form toxic species [30]. Furthermore, despite their proven antioxidant activity, CeO_2NPs can induce oxidative stress [31]. Therefore, an efficient strategy could be the encapsulation of CeO_2NPs to prevent their immediate release and to decrease their toxicity. Indeed, Weaver et al. demonstrated that this cytotoxicity can be eliminated by embedding CeO_2NPs into a polymer (e.g., hydrogel) matrix, this system allows to modulate the oxidant activity of CeO_2NPs, but also to enhance the antimicrobial and antioxidative properties of this material [32]. However, it is believed that the surfactant and polymer change the surface charge of CeO_2NPs, forming a complex with the metal, filling the oxygen vacancy and prevents the oxidation state [33].

In this work, a new antibiofilm system is described, based on CeO_2NPs synthetized by W/O microemulsion method [34], and encapsulated in the polymeric matrix polylactic-co-glycolic acid (PLGA) micelles, through single emulsion/solvent method [35]. The polymeric system was characterized in terms of size, surface charge, morphology and chemical speciation through XPS. The formulations were then incorporated in two types of natural and biodegradable films, namely gelatine or maize starch, to obtain the final antibiofilm systems. The low cost, high availability, and diverse functionalities like water retention and tailorable viscosity [36] of gelatine and starch are highly desirable for their use and processability in food industry. Moreover, starch itself is an important food ingredient and, by physicochemical modification, can possess good film-forming and emulsification properties [37,38]. Finally, the preparation, characterization, and antimicrobial properties of these films are discussed in the paper, in view of their application in food packaging field.

2. Experimental

2.1. Materials

The chemical compounds used for the synthesis of CeO_2NPs and their encapsulation in micelles were $Ce(NO_3)_3$*$6H_2O$ (Sigma Aldrich Mw: 432,22 g/mol), Ammonia 30 % (v/v) (Panreac AppliChem Barcelona, Spain), Cetyl Trimethyl Ammonium Bromide 99 % (CTAB), 1-butanol (min. 99 %) and hydrochloric acid 38 % (HCl), ethanol (95 %), 1-Hexanol, and 1-Butanol were purchased by Sigma-Aldrich (Madrid, Spain). Micelles were formed using PLGA (LG 50:50, Mw24–38 kDa) purchased from Sigma Chemical Co. (Steinheim, Germany). Polyvinyl alcohol (PVA) (Mw 30–70 kDa), phosphatidylcholine (PC) from soybean (Phospholipon 90G) was obtained from Lipoid (Koln, Germany). Gelatine films were prepared using gelatine from porcine skin (Sigma-Aldrich ref. G1890) and glycerol (Sigma-Aldrich 99.5 % ref. G7893). Starch films were prepared with Maize starch with 0.25 % moisture and a branching (α-1,4)/(α-1,6) ratio of 15.2 purchased from Cerestar-AKV I/S (Denmark). The *E. coli* strain used for the antimicrobial activity test was kindly given by the Dairy Research Institute of Asturias (Instituto de Productos Lácteos de Asturias, IPLA-CSIC), Asturias, Spain.

2.2. Synthesis of cerium nanoparticles

CeO_2NPs were produced with the W/O microemulsion method according to previous studies [34,35]. CTAB was used as surfactant, 1-butanol as cosurfactant, and 1-hexanol as continuous oily phase. CTAB/1-butanol weight ratio was kept constant to 3:2. In the aqueous phase two different $Ce(NO_3)_3$*$6H_2O$ concentrations were used, 0.5 and 1 M. After the homogenization of organic phase with magnetic stirrer, the aqueous phase was added. The two formulations of the W/O microemulsions used for the synthesis are shown in Table S1. The microemulsions were left to rest for a few minutes until the appearance was totally translucid indicating the microemulsion formation.

Afterwards, a co-precipitation method was used in order to produce the CeO_2NPs. For this purpose, an ammonia solution, 30 % (v/v), was added dropwise upon vigorous stirring. Once a dark pink precipitate appeared, the solution was left for two hours under gentle magnetic stirring. The microemulsion was purified by centrifugation at a temperature of 20 °C at 10000 rpm for 15 min and the pellet was resuspended with a mixture of water and absolute ethanol 25 % v/v twice, and then with water for two times more (see Fig. 1a).

2.3. Encapsulation in PLGA micelles

CeO_2NPs were encapsulated in micelles by a single emulsion/solvent method [35] as depicted in Fig. 1b. 20 mg of PLGA was dissolved in 2 mL of organic phase consisting of 12.5 % (v/v) methanol in chloroform. 6 mL of aqueous phase was prepared with 12 mg PC and 1 % PVA (w/v) in which 200 μL of CeO_2NPs were let to dissolve for 2 h. Then both phases were mixed to form an O/W emulsion under continuous sonication with the amplitude of 70 % for 5 min in the ice bath. The emulsion was kept under magnetic stirring overnight to allow evaporation of the organic solvent. The final result was PLGA micelles encapsulating the CeO_2NPs.

2.4. Preparation of gelatine and starch films

1 g of gelatine derived from porcine skin and 0.35 g of glycerol were directly added to 10 mL of NPs suspension to obtain gelatine films. The mixtures were then placed in a water bath at 60 °C for 30 min to ensure complete gelatine dissolution. Once dissolved, the solutions were poured into Petri dishes and allowed to dry in an oven at 40 ∘C for 24 h [39].

Maize starch films were prepared in a similar way, but in this case the amount of starch used was 0.5 g and mixed in 0.1 g of glycerol in 10 mL of the sample. The mixture was dissolved at 85 °C and then dried at 40 °C in the oven for 24 h.

Several types of films were produced: (i) just films as blank, (ii) films with free CeO_2NPs, (iii) films with empty micelles and (iv) films with CeO_2NPs encapsulated in micelles (see Fig. 2).

2.5. Characterization

CeO_2NPs suspensions were characterized in terms of size distribution, average size, polydispersity index (PDI), and zeta-potential through dynamic light scattering (DLS) on a Zetasizer NanoZS series (Malvern Instruments Ltd., Malvern, UK). To study the morphology of each formulation, negative staining transmission electron microscopy (NS-TEM) was employed. A JEOL-2000 Ex II Transmission Electron Microscope from Tokyo, Japan was used for this purpose. Films morphology was observed using a scanning electron microscope (SEM) (JSM-5600, JEOL, Peabody, MA, USA) analysing the surface and cross-sections. Films were cut into squares and placed on stubs, after gold metallization. X-ray Photoelectron Spectroscopy analyses were performed with a Versa Probe II Scanning XPS Microprobe spectrometer (Physical Electronics GmbH). The suspensions were drop casted on metal foil and the films were placed on silicon foil. A monochromatized AlKα source with an x-ray spot size of 200 μm and a power of 49.2 W was utilized. Wide scans and detailed spectra were acquired in Fixed Analyzer Transmission (FAT) mode with a pass energy of 46.95 eV. An electron gun was used for charge compensation (1.0 V 20.0 μA). All binding energies were referenced to C1s at 284.8 ± 0.1 eV for adventitious hydrocarbon. Data processing were performed using MultiPak software v. 9.9.0.8, 2018.

2.6. Agar well diffusion method

Antimicrobial activity tests were performed in vitro on *E. coli* by the agar well diffusion method evaluating the inhibition zones. Bacteria cultures (100 μL) were inoculated in 15 mL of nutrient agar medium, poured into Petri dishes, and allowed to solidify at 37 °C. Using a sterile glass tube of 1 cm diameter, holes were carefully made in these agar

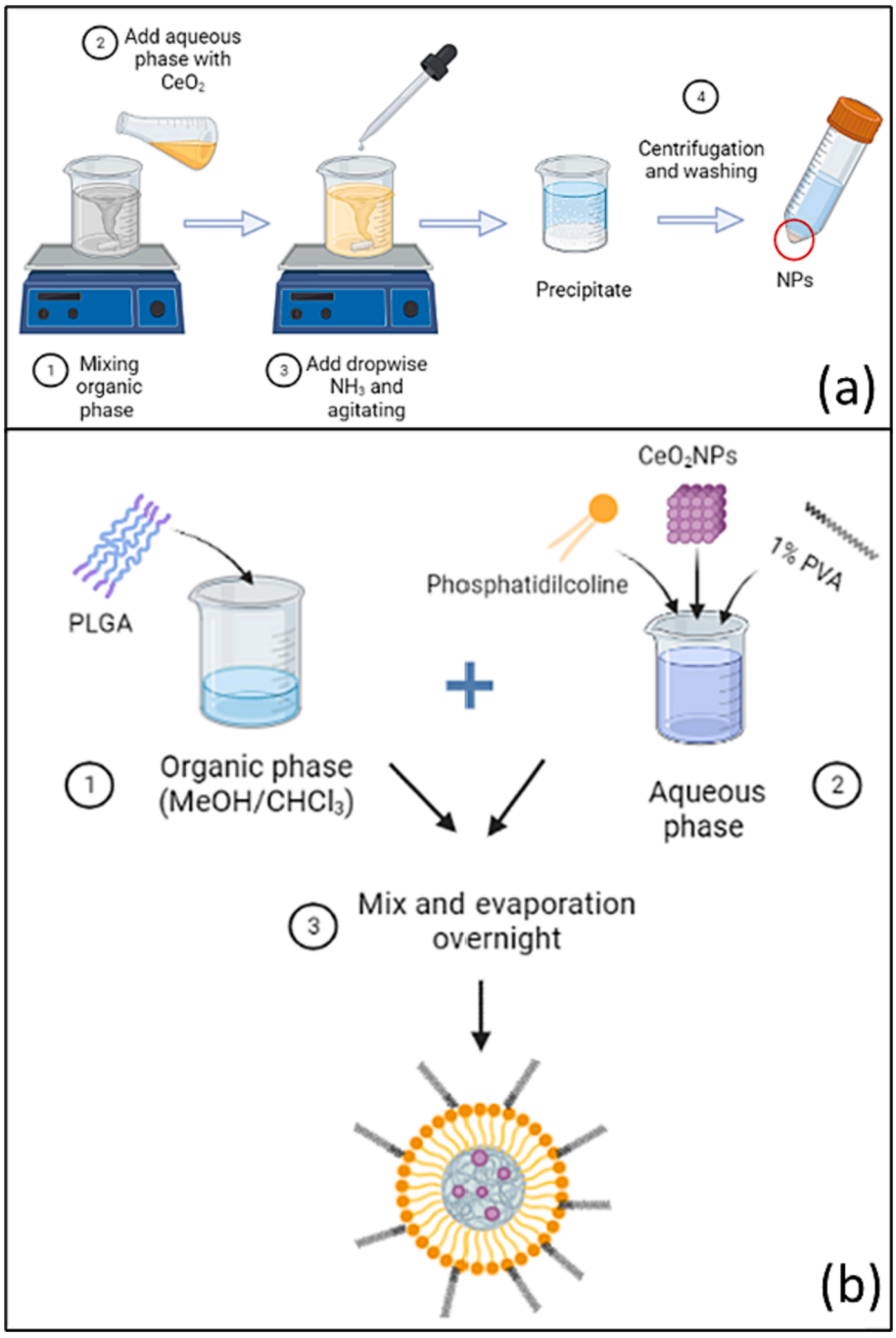

Fig. 1. (a) Scheme of W/O microemulsion and co-precipitation method for CeO_2NPs preparation. (b) Encapsulation of CeO_2NPs in PLGA micelles.

cultures. The films were dissolved in the oven at 34 °C for 24 h and then subsequently placed into each hole in the plate. These plates were then placed in an incubator at 37 °C for 24 h. The appearance of circular areas devoid of bacterial growth around the wells in the plates indicated the antimicrobial effectiveness of the films tested. The diameter of the inhibition zones was measured, and the average value was calculated based on triplicate experiments.

3. Results and discussion

3.1. Characterization of CeO_2NPs suspensions and CeO_2NPs encapsulated in PLGA micelles

Size distribution and surface charge of CeO_2NPs suspensions and PLGA micelles are reported in Table 1. The average size of empty PLGA micelles is around 60 nm with a low and negative surface charge. The CeO_2NPs alone are larger in size, and it was observed that after the addition of CeO_2NPs in PLGA micelles, the hydrodynamic size of the hybrid system increased up to 100–200 nm, pointing out the effective encapsulation. Additionally, the zeta potential of cerium nanoparticles is high and positive for both formulations, ~60–90 mV, indicating a stability of particles by electrostatic repulsion. When the particles are encapsulated in PLGA micelles the zeta potential becomes close to zero as in the case of empty micelles. This could be detrimental in terms of micelles aggregation, but the final dispersion into the films was able to overcome this point (see below).

Fig. 3 reports the TEM characterization of NPs and micelles. In Fig. 3a TEM images show the morphology of CeO_2NPs and PLGA empty

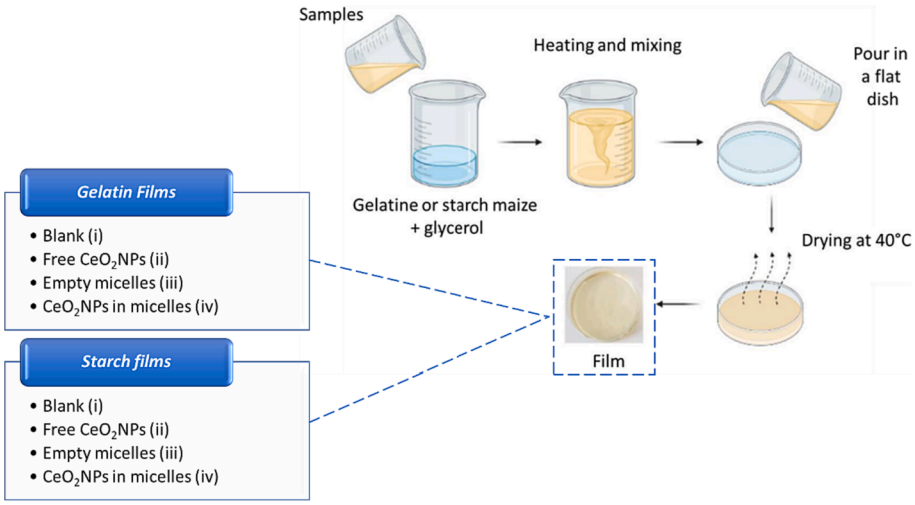

Fig. 2. Scheme of films preparation.

Table 1
Size and zeta-potential of empty micelles, cerium nanoparticles (formulations A and B), and cerium nanoparticles in PLGA micelles.

Samples	Size (nm)	Z-potential (mV)
PLGA micelles	60 ± 4	−0.3 ± 0.5
CeO_2NPs (A)	247 ± 4	63.8 ± 0.1
CeO_2NPs (B)	149 ± 8	89.7 ± 3.3
PLGA micelles + CeO_2NPs (A)	322 ± 44	−1.9 ± 0.2
PLGA micelles + CeO_2NPs (B)	156 ± 6	−1.1 ± 0.1

micelles. PLGA micelles appear to be well separated, round-shape and their size is around 50–60 nm, in agreement with DLS measurements. CeO_2NPs images show the presence of aggregates formed by small particles (ca 10 nm) in both cases A and B. When both CeO_2NPs A and B are encapsulated, the formation of micelles and the presence of the NPs inside them was clearly identified form TEM images reported in Fig. 3b and 3c. Nevertheless, the NPs encapsulation yielded partially agglomerated micelles.

3.2. Morphological characterization of the films

All the gelatine-based and maize starch-based films were characterized by SEM. Figure S1 shows the images of the transversal cut sections obtained for gelatine films (left) and maize starch films (right). In the case of gelatine films, the blank (Fig. S1a) does not differ in structure from the ones containing micelles and nanoparticles. All films present a smooth and homogeneous aspect. The film with micelles and CeO_2NPs B (f) shows a difference in structure, probably due to some issues in the film cutting. All the maize starch films have a different texture with respect to the gelatine ones, especially when micelles and particles are incorporated: the latter show less homogeneous systems. In addition, it

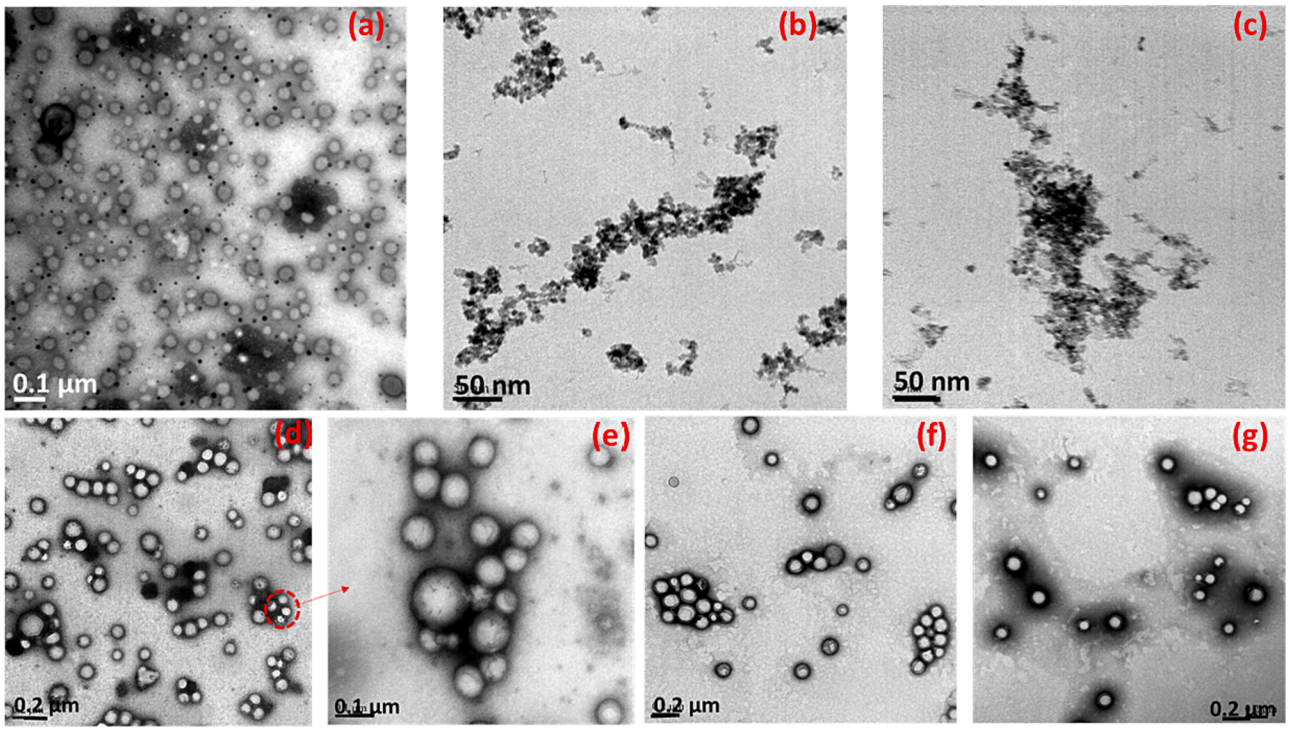

Fig. 3. TEM images of empty micelles (a), CeO_2NPs A (b), CeO_2NPs (c), PLGA micelles with the two formulations of CeO_2NPs A (d) (e), and CeO_2NPs B (f) (g).

was noted from the SEM images that the thickness of the gelatine film is 261 μm, while that of the maize starch is 126 μm.

3.3. X-ray Photoelectron Spectroscopy (XPS) of CeO_2NPs

CeO_2NPs were analysed by XPS, for elemental identification and chemical speciation of colloids with two different Ce concentrations. From the high resolution spectral region of each element, the elemental atomic percentages have been calculated for both the synthesis of CeO_2NPs A and CeO_2NPs B and the values are reported in Fig. 4 (inset).

As expected on the base of the stoichiometry, the elements found on the surface of both samples are carbon, oxygen, and cerium. Moreover, similar %Ce are detected on CeO_2NPs A and CeO_2NPs B despite the amount of surfactant used in the two different methods. The carbon and the oxygen amount is high in all the samples, according to the emulsion and surfactant composition. Nitrogen and bromine, coming from CTAB surfactant, are hardly detectable on the surface of both the samples, and their amount is below the limit of detection. This experimental evidence can be explained by a loss of the capping agent during all the steps of the NPs synthesis.

To investigate Ce chemical environment, the curve fitting procedure was applied to Ce3d and O1s XP spectral regions. In particular, due to the complex structure of Ce3d, this region was thoroughly interpretated on the basis of the literature [40–43]. The detailed analysis of the Ce3d multiplet splitting allowed to identify the oxidation state of the core of the NPs, on the basis of the binding energy (BE) values of each peak component. Literature confirms the natural coexistence in oxides of both Ce (III) an (IV) due to Ce property of changing its oxidation state continuously [42]. On the base of the fitting parameters reported in [42], the Ce3d XP spectra of CeO_2NPs A and B have been curve-fitted and a typical result is reported in Fig. 4. The same multiplet splitting was obtained for the curve-fitted XP spectrum of CeO_2NPs B. Therefore, the discussion on the Ce chemical speciation is valid for both the samples.

The line shape of Ce3d spectrum is clearly a combination of the Ce (III) and Ce (IV) multiplet splitting [42,43]; moreover, on the base of the curve fitting results of Fig. 4, it is possible to observe the presence of v^0, v^I, and u^I typical peak components of Ce (III), and the peak u^{III} at 916.7 ± 0.1 eV, typical of Ce (IV). The relative abundances of peak components u^I, v^0 and v^{II} have been calculated and an estimation of Ce (III) percentage has been derived (columns 2 and 3, Table S2).

The confirmation about Ce(III) presence was obtained by O1s XP spectra curve-fitting (Figure S2), in order to derive the relative abundances of oxygen component bound to cerium. The O1s spectral region showed the presence of five peak components, attributed to the following oxygen chemical environments according to the BE values. The first peak at BE = 529.2 ± 0.1 eV is ascribable to oxygen of CeO_2, and the second at BE = 530.7 ± 0.1 eV ascribable to oxygen of Ce_2O_3, both indicating the presence of cerium oxides [44]. The peak components at higher BE values (532 – 534 eV) are attributable to organic oxygen, due to the natural surface contamination. Through the values obtained, it was possible to calculate the inorganic oxygen percentages and O/Ce ratios: for both oxides it is close to the stoichiometric value. All the results can be found in Table S2.

3.4. X-ray Photoelectron Spectroscopy (XPS) of gelatine and maize starch films

After characterizing the CeO_2NPs A and B, it was concluded that for both nanoparticles the speciation is similar, therefore the following results about the analysis of gelatine and starch films are presenting taking into account only the CeO_2NPs A.

The systems studied were the bare biodegradable polymer films, PLGA micelles, CeO_2NPs A encapsulated in PLGA micelles, the polymer films containing CeO_2NPs A or empty PLGA micelles, and the films embedding CeO_2NPs A encapsulated in PLGA micelles. In Table 2 are resumed the values of the elemental atomic percentages measured for all the samples.

The elements found on the surface of gelatine film are carbon, nitrogen, oxygen according to its organic components. Elements found for

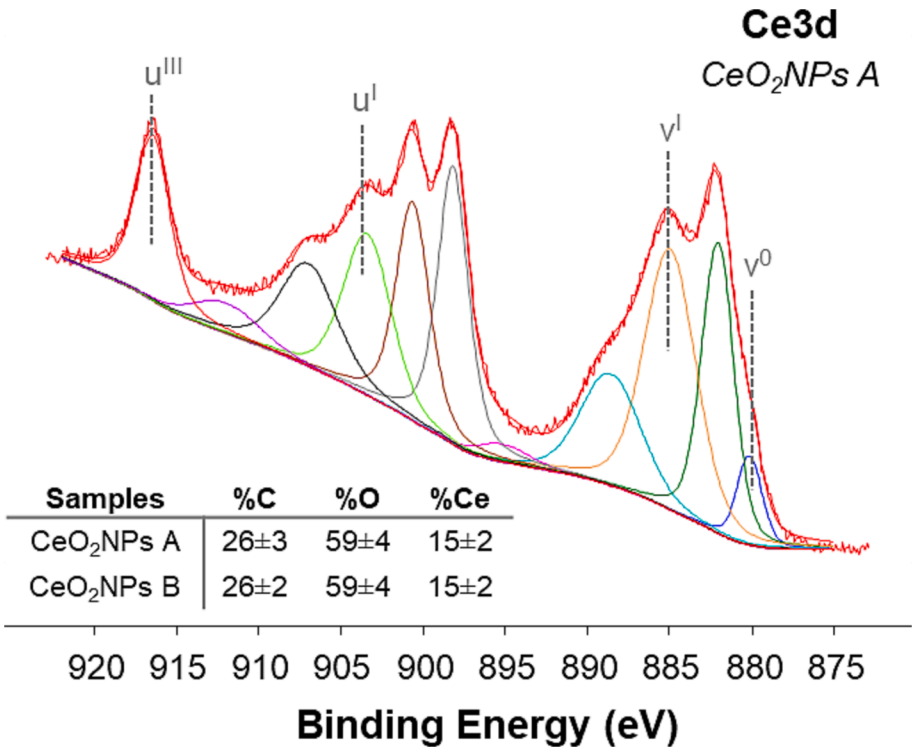

Fig. 4. Curve fitted Ce3d XP spectrum of CeO_2NPs A. Inset: Elemental atomic percentages of for CeO_2NPs A and CeO_2NPs B. The values are reported as mean values ± 1S (n = 3).

Table 2
Elemental atomic percentages of each element present in all the prepared samples. The values are reported as mean values ± 1S (n = 3).

Samples	%C	%N	%O	%Ce	%P
PLGA micelles	75.0 ± 1.1	0.9 ± 0.5	23.2 ± 1.0		0.9 ± 0.5
CeO_2NPs + PLGA	73.6 ± 0.6	1.2 ± 0.5	24.1 ± 0.6	0.1 ± 0.5	1.0 ± 0.5
Gelatine film	69.7 ± 1.5	11.9 ± 0.9	18.4 ± 0.6		
PLGA in gelatine film	76.1 ± 1.4	5.2 ± 0.5	18.3 ± 0.7		0.4 ± 0.5
CeO_2NPs in gelatine film	68.0 ± 1.2	12.7 ± 0.5	19.2 ± 1.0	n.d.	
CeO_2NPs + PLGA in gelatine film	68.0 ± 1.6	11.5 ± 0.8	20 ± 1	n.d.	0.4 ± 0.5
Maize starch film	63 ± 2	2.5 ± 0.5	34 ± 2		
PLGA in maize starch film	67.5 ± 0.7	0.8 ± 0.5	31.4 ± 0.7		0.3 ± 0.5
CeO_2NPs in maize starch film	66 ± 2	1.2 ± 0.5	32 ± 2	0.1 ± 0.5	
CeO_2NPs + PLGA in maize starch film	72.2 ± 0.7	0.5 ± 0.5	27.2 ± 0.9	0.1 ± 0.5	–

PLGA micelles are carbon, oxygen, nitrogen and phosphorous, expected for the compounds added in the synthesis (polymers and phospholipids). All these elements are found also in CeO_2NPs A in gelatine film and micelles with CeO_2NPs A in gelatine film, but cerium is visible only in non-embedded CeO_2NPs + PLGA.

The surface of the samples is mainly organic, as confirmed by carbon percentage; even if the presence of cerium is detected on the surface of gelatine film embedding free CeO_2NPs or encapsulated in micelles, it is as low as 0.01 ± 0.1 at%. To have a clearer idea and more information about how the surface is made, the analysis of the C1s signal shape and curve fitting was done for all the systems (Fig. 5).

From Fig. 5 we can see how C1s signal of PLGA micelles in gelatine film (in the left) is a combination of PLGA and gelatine, as evident from the presence of the peak component at BE = 287.5 ± 0.3 eV (yellow line) from the gelatine and the peak component at BE = 288.9 ± 0.1 eV (cyan line) from PLGA. C1s spectrum of CeO_2NPs A in PLGA micelles (e) has a line shape similar to C1s of PLGA (b): this suggests that CeO_2NPs A are not on the surface, but probably deeper and encapsulated. C1s of CeO_2NPs A in PLGA micelles incorporated in gelatine film (f) resembles gelatine film C1s line shape, indicating that CeO_2NPs-PLGA micelles are incorporated into the gelatine. On the base of these results, it can be hypothesized that empty and loaded PLGA micelles have different density, so that the NPs-PLGA go deeper into the gelatine because of the higher density. The same approach was used for the analysis of maize starch films (Table 2). The elemental composition was expected on the base of samples stoichiometry. In comparison with gelatine films, in maize starch film the presence of CeO_2NPs A has been detected on the surface. In order to observe the behaviour of nanoparticles and micelles

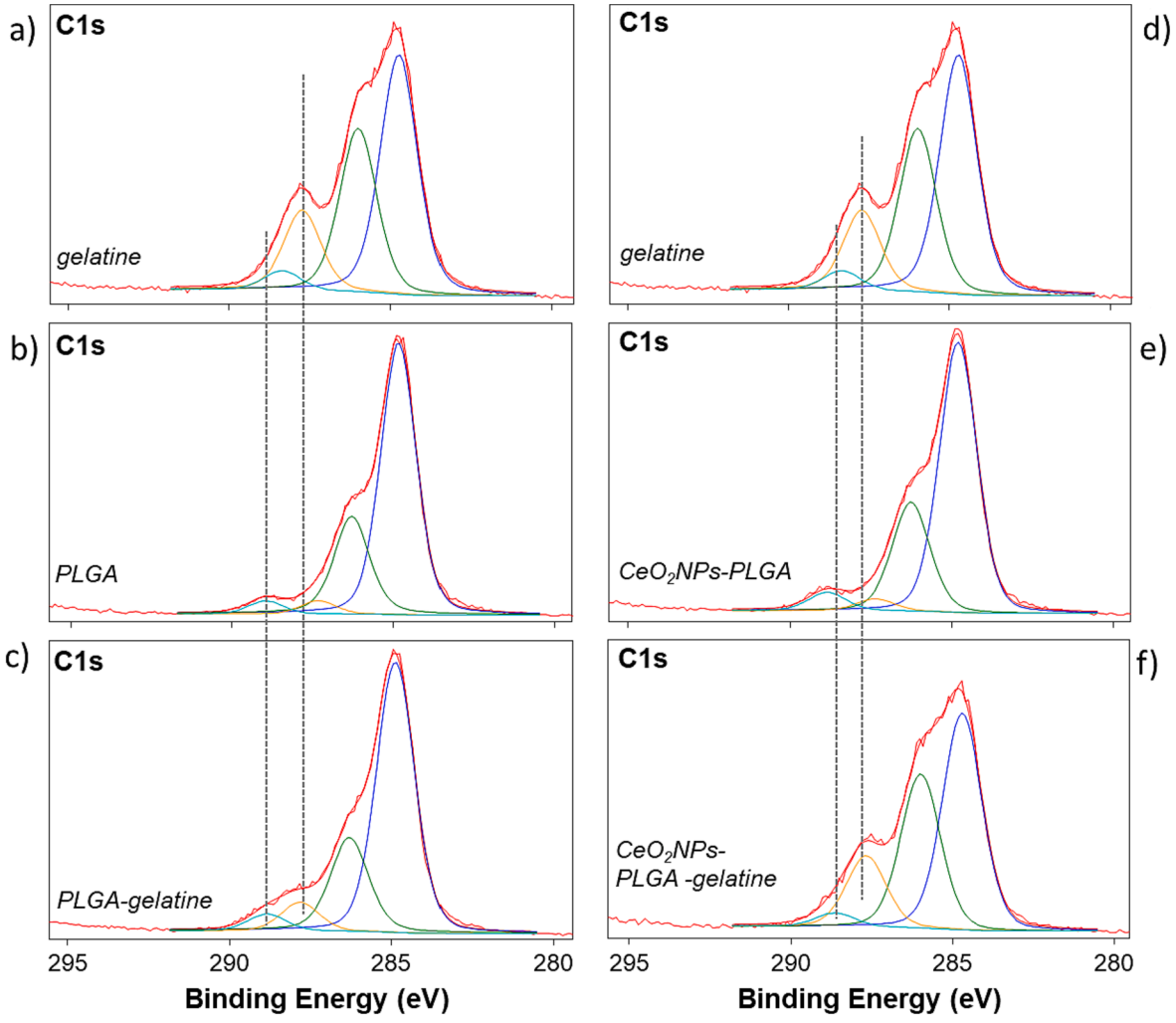

Fig. 5. Curve fitted C1s XP spectra of gelatine film alone, PLGA micelles, PLGA micelles added in gelatine film, CeO_2NPs encapsulated in PLGA micelles and CeO_2NPs in PLGA micelles incorporated in gelatine film.

on the surface of this type of film C1s was curve fitted for all the systems and the results are reported in Fig. 6 (a-f). The C1s of PLGA micelles in maize starch film (in the left) is an evident combination of PLGA and maize starch as it shown are present both peaks (dash lines). In the left the C1s of CeO_2NPs in PLGA micelles incorporated in maize starch film is still a mix of the two carbons, indicating that the micelles are on the surface, for this reason the cerium of CeO_2NPs was detected. To summarize by looking at the carbon XP spectra of the two types of films and comparing them with the carbon of micelles and nanoparticles, it can be said that while in gelatine films the micelles-nanoparticle system is not noticeable on the surface, in the starch film the carbon resembles a combination of all components of the system indicating that micelles and nanoparticles are present on the surface. Clearly, the higher density of CeO_2NPs-PLGA micelles did not affect their surface availability because of the higher crosslinking degree of maize starch films.

4. Antimicrobial Test: Proof of concept

Cerium nanoparticles are well known to possess antimicrobial and antibiofilm activity, especially against gram negative bacteria, like E. Coli, commonly used for testing the antimicrobial properties of food-packaging materials [45]. Therefore, initial studies were conducted on the bacterial planktonic phase to determine if the films could be used for the proposed application. The antimicrobial activity of gelatin and starch films systems was studied and compared using agar well diffusion method as depicted in Fig. 7.

From Fig. 7A we observe that gelatin films without cerium nanoparticles (1) do not show antimicrobial activity, as evident from the absence of any halo around the well. A slight non-homogeneous halo is visible in the second well, containing gelatin films embedding PLGA micelles, which have a structure capable of penetrating or disrupting bacterial cell walls [46]. The halo becomes clear around well (3) with gelatin film including the CeO_2NPs and with well (4) when gelatin films contained CeO_2NPs encapsulated in PLGA micelles. The third halo has a diameter of 1.1 cm and the fourth of 1 cm. Also in this case the halo is non-homogenous, maybe depending on the concentration of the hybrid structure, the density of the bacteria and how the antimicrobial compounds diffuses in the agar plate [47].

Differently than expected, starch films showed no antimicrobial activity (Fig. 7B), as the bacteria grew around the well and across the entire plate. Despite the higher surface availability of Ce nanoparticles on starch systems than gelatin ones, a lower effect was obtained. This behaviour can be explained by dose-dependent nature of the cerium nanoparticles on *E. coli* [45], indicating the necessity of a higher concentration of cerium nanoparticles, in particular because they are also encapsulated in micelles. Additionally, previous studies utilizing starch as the main compound in food-packaging films revealed a reduced antimicrobial activity of compounds embedded in such films compared to others [48], probably because of the crosslinking that reduces the interaction and the adsorption of the microorganisms.

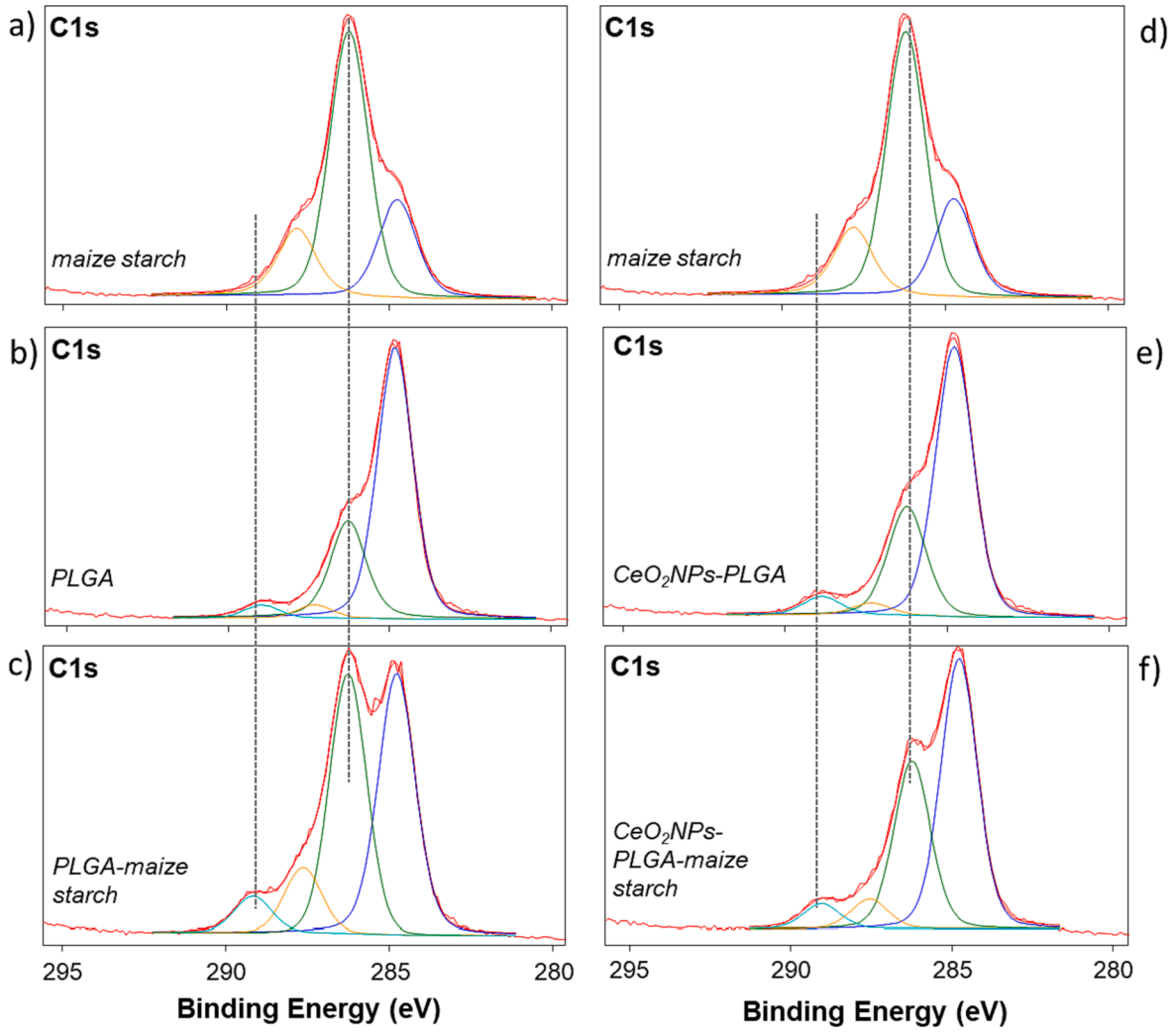

Fig. 6. Curve fitted C1s XP spectra of maize starch film alone, PLGA micelles, PLGA micelles added in maize starch film, CeO_2NPs encapsulated in PLGA micelles and CeO_2NPs in PLGA micelles incorporated in maize starch film.

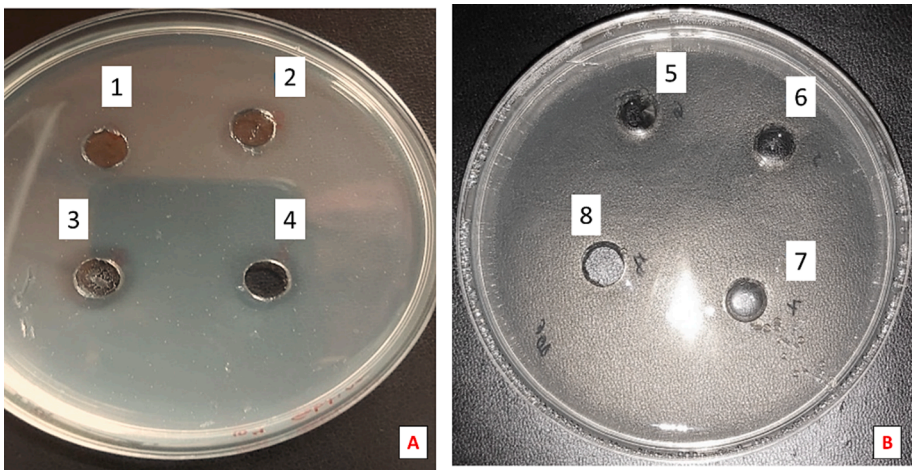

Fig. 7. Agar plates containing: A) dissolved gelatin films and B) dissolved starch films. In A) the well (1) is the blank gelatin film, the well (2) is gelatin film with PLGA micelles, the (3) is gelatin film with CeO_2NPs and (4) is gelatin film with CeO_2NPs encapsulated in PLGA micelles. In B) the well (5) is the blank starch film, (6) is starch film with PLGA micelles, (7) is starch film with CeO_2NPs and (8) is starch film with CeO_2NPs encapsulated in PLGA micelles.

5. Conclusions

The novel antibacterial properties of CeO_2NPs and their applications in material and life science inspired this work on new nano-systems aiming at exploiting biochemical and physical properties of our hybrid materials. The emulsion-precipitation method followed by polymer and micelles encapsulation was chosen among the different synthesis methods available in literature for CeO_2NPs, because it ensured greater stability and lower Ce oxidation phenomena.

From the results obtained from DLS and TEM, we concluded that good encapsulation of nanoparticles within micelles has been achieved. Surface chemical speciation demonstrated the protection of stabilised CeO_2NPs from its oxidation. From XPS results we also observed that CeO_2NPs-PLGA systems are easily incorporated into the selected biodegradable films and are more available on the surface when starch matrix is used, due to its crosslinked structure.

On the basis of our findings we can conclude that CeO_2NPs-PLGA systems were successfully synthesised and characterised as well as easily incorporated in sustainable food-packing films, made of gelatine or starch, representing good candidates for antibiofilm applications.

Moreover, the first antimicrobial tests proved that gelatin still remains a biodegradable and edible compounds good for forming food-packaging films and facilitating the embedding and release of antimicrobial compounds. However, to enhance effectiveness, the concentration of the hybrid nanostructures needs to be increased and rigorously tested against both planktonic phase bacteria and biofilms.

CRediT authorship contribution statement

Verdiana Marchianò: Data curation, Investigation, Writing – original draft. **Maria Matos:** Conceptualization, Methodology. **Ismael Marcet:** Investigation, Methodology. **M. Carmen Blanco-López:** Supervision, Funding acquisition, Project administration. **Gemma Gutiérrez:** Conceptualization, Project administration, Supervision, Writing – review & editing. **Nicola Cioffi:** Funding acquisition, Supervision. **Nicoletta Ditaranto:** Conceptualization, Project administration, Supervision, Writing – review & editing.

Declaration of competing interest

The authors declare that they have no known competing financial interests or personal relationships that could have appeared to influence the work reported in this paper.

Data availability

Data will be made available on request.

Acknowledgement

This work is part of a project that has received funding from the EU Horizon 2020 research and innovation program under the Marie Sklodowska-Curie Grant Agreement No. 813439 (Break Biofilms). This research was also funded by the Ministerio de Economía y Competitividad (MINECO, Spain), grant number PID2019-105311RB-I00 and was also co-financed by Consejería de Educación y Ciencia del Principado de Asturias (AYUD/2021/52132).

Appendix A. Supplementary data

Supplementary data to this article can be found online at https://doi.org/10.1016/j.molliq.2024.124215.

REFERENCES

[1] M. Yadav, P. Sharma, N.S. Chauhan, Metal oxide–based heterostructures for antimicrobial activity, Met. Oxide-Based Heterostruct. Fabr. Appl. (2022) 535–570, https://doi.org/10.1016/B978-0-323-85241-8.00008-6.
[2] A.M. Negrescu, M.S. Killian, S.N.V. Raghu, P. Schmuki, A. Mazare, A. Cimpean, Metal Oxide Nanoparticles: Review of Synthesis, Characterization and Biological Effects, J. Funct. Biomater. 13 (2022), https://doi.org/10.3390/JFB13040274.
[3] E. Barker, J. Shepherd, I.O. Asencio, The Use of Cerium Compounds as Antimicrobials for Biomedical Applications, Mol. 2022, Vol. 27, Page 2678. 27 (2022) 2678. Doi: 10.3390/MOLECULES27092678.
[4] J. Raczkowska, Y. Stetsyshyn, K. Awsiuk, M. Brzychczy-Włoch, T. Gosiewski, B. Jany, O. Lishchynskyi, Y. Shymborska, S. Nastyshyn, A. Bernasik, H. Ohar, F. Krok, D. Ochońska, A. Kostruba, A. Budkowski, "Command" surfaces with thermo-switchable antibacterial activity, Mater. Sci. Eng. c. 103 (2019) 109806, https://doi.org/10.1016/J.MSEC.2019.109806.
[5] Y. Tang, Z. Qin, S. Yin, H. Sun, Transition metal oxide and chalcogenide-based nanomaterials for antibacterial activities: an overview, Nanoscale. 13 (2021) 6373–6388, https://doi.org/10.1039/D1NR00664A.
[6] K.R. Singh, V. Nayak, J. Singh, A.K. Singh, R.P. Singh, Potentialities of bioinspired metal and metal oxide nanoparticles in biomedical sciences, RSC Adv. 11 (2021) 24722–24746, https://doi.org/10.1039/D1RA04273D.
[7] J. Bi, C. Mo, S. Li, M. Huang, Y. Lin, P. Yuan, Z. Liu, B.o. Jia, X.u. Shuaimei, Immunotoxicity of metal and metal oxide nanoparticles: from toxic mechanisms to metabolism and outcomes, Biomater. Sci. 11 (2023) 4151–4183, https://doi.org/10.1039/D3BM00271C.
[8] K.R. Singh, V. Nayak, T. Sarkar, R. Pratap Singh, Cerium oxide nanoparticles: properties, biosynthesis and biomedical application, (2020). Doi: 10.1039/d0ra04736h.
[9] V. Marchianò, M. Salvador, A. Moyano, G. Gutiérrez, M. Matos, S. Yáñez-Vilar, Y. Piñeiro, J. Rivas, J.C. Martínez-García, D. Peddis, M.C. Blanco-López, M. Rivas, N. Ditaranto, N. Cioffi, Electrodecoration and Characterization of

Superparamagnetic Iron Oxide Nanoparticles with Bioactive Synergistic Nanocopper: Magnetic Hyperthermia-Induced Ionic Release for Anti-Biofilm Action, Antibiotics. 10 (2021) 119, https://doi.org/10.3390/antibiotics10020119.
[10] M.C. Sportelli, R.A. Picca, N. Cioffi, Nano-Antimicrobials Based on Metals, Nov. Antimicrob. Agents Strateg. (2014) 181–218. Doi: 10.1002/9783527676132.CH8.
[11] S.I. Hossain, E.A. Kukushkina, M. Izzi, M.C. Sportelli, R.A. Picca, N. Ditaranto, N. Cioffi, A Review on Montmorillonite-Based Nanoantimicrobials: State of the Art, Nanomaterials. 13 (2023), https://doi.org/10.3390/NANO13050848.
[12] M. Izzi, M.C. Sportelli, L. Torsi, R.A. Picca, N. Cioffi, Synthesis and Antimicrobial Applications of ZnO Nanostructures: A Review, ACS Appl. Nano Mater. (2023), https://doi.org/10.1021/ACSANM.3C01432.
[13] D. Longano, N. Ditaranto, L. Sabbatini, L. Torsi, N. Cioffi, Synthesis and Antimicrobial Activity of Copper Nanomaterials (2014), https://doi.org/10.1007/978-3-642-24428-5_3.
[14] M.A. Pérez-Díaz, G. Prado-Prone, A. Díaz-Ballesteros, M. González-Torres, P. Silva-Bermudez, R. Sánchez-Sánchez, Nanoparticle and nanomaterial involvement during the wound healing process: an update in the field, J. Nanoparticle Res. 25 (2023), https://doi.org/10.1007/S11051-023-05675-9.
[15] S.A. Mir, V. Shrotriya, T.I. Al-Muhimeed, M.A. Hossain, B. Zaman, Metal and metal oxide nanostructures applied as alternatives of antibiotics, Inorg. Chem. Commun. 150 (2023) 110503, https://doi.org/10.1016/j.inoche.2023.110503.
[16] H.A. Hemeg, Nanomaterials for alternative antibacterial therapy, Int. J. Nanomedicine. 12 (2017) 8211–8225, https://doi.org/10.2147/IJN.S132163.
[17] K. Ashwini, Cerium Oxide Nanoparticles: Synthesis, Characterization and Study of Antimicrobial Activity, Artic. J. Nanomater. Mol. Nanotechnol. (2017), https://doi.org/10.4172/2324-8777.1000219.
[18] N.P. Yerriboina, S. Sahir, S.-Y. Han, N. Aqilah, M. Fadzil, M. Hasbi, A.B. Rahim, G. P. Maniam, Brief review of ceria and modified ceria: synthesis and application Cerium Oxide Slurries in CMP, Electrophoretic Mobility and Adsorption Investigations of Ceria/silicate Interaction Preuchsuda Suphantharida and Kwadwo Osseo-Asare-the Adhesion and Removal Mechanism of Ceria Particles for STI Post-CMP Cleaning Process Brief Review of Ceria and Modified Ceria: Synthesis and Application (2018), https://doi.org/10.1088/2053-1591/aad2b5.
[19] N. Thakur, P. Manna, J. Das, Synthesis and biomedical applications of nanoceria, a redox active nanoparticle, J. Nanobiotechnology 2019 171. 17 (2019) 1–27. Doi: 10.1186/S12951-019-0516-9.
[20] O.L. Pop, A. Mesaros, D.C. Vodnar, R. Suharoschi, F. Tăbăran, L. Mageruşan, I.S. Tódor, Z. Diaconeasa, A. Balint, L. Ciontea, C. Socaciu, Cerium Oxide Nanoparticles and Their Efficient Antibacterial Application In Vitro against Gram-Positive and Gram-Negative Pathogens, Nanomater. 2020, Vol. 10, Page 1614. 10 (2020) 1614. Doi: 10.3390/NANO10081614.
[21] M.A. Dar, R. Gul, P. Karuppiah, N.A. Al-Dhabi, A.A. Alfadda, Antibacterial Activity of Cerium Oxide Nanoparticles against ESKAPE Pathogens, Cryst. 2022, Vol. 12, Page 179. 12 (2022) 179. Doi: 10.3390/CRYST12020179.
[22] A.B. Shcherbakov, V. V. Reukov, A. V. Yakimansky, E.L. Krasnopeeva, O.S. Ivanova, A.L. Popov, V.K. Ivanov, CeO2 Nanoparticle-Containing Polymers for Biomedical Applications: A Review, Polym. 2021, Vol. 13, Page 924. 13 (2021) 924. Doi: 10.3390/POLYM13060924.
[23] M. Hosseini, M. Mozafari, Cerium Oxide Nanoparticles: Recent Advances in Tissue Engineering, Mater. 2020, Vol. 13, Page 3072. 13 (2020) 3072. Doi: 10.3390/MA13143072.
[24] O.A. Legon'kova, T.A. Ushakova, I.P. Savchenkova, N. V. Perova, M.S. Belova, A.A. Torkova, A.E. Baranchikov, O.S. Ivanova, A.I. Korotaeva, V.K. Ivanov, Experimental Study of the Effects of Nanodispersed Ceria on Wound Repair, Bull. Exp. Biol. Med. 162 (2017) 395–399, https://doi.org/10.1007/S10517-017-3624-2/METRICS.
[25] M.M.T. Jansman, L. Hosta-Rigau, Cerium- and Iron-Oxide-Based Nanozymes in Tissue Engineering and Regenerative Medicine, Catal. 2019, Vol. 9, Page 691. 9 (2019) 691. Doi: 10.3390/CATAL9080691.
[26] D.A. Pelletier, A.K. Suresh, G.A. Holton, C.K. McKeown, W. Wang, B. Gu, N. P. Mortensen, D.P. Allison, D.C. Joy, M.R. Allison, S.D. Brown, T.J. Phelps, M. J. Doktycz, Effects of engineered cerium oxide nanoparticles on bacterial growth and viability, Appl. Environ. Microbiol. 76 (2010) 7981–7989, https://doi.org/10.1128/AEM.00650-10/SUPPL_FILE/DOKTYCZ_SUPPLEMENTAL_MATERIAL.DOC.
[27] G. Sharmila, C. Muthukumaran, H. Saraswathi, E. Sangeetha, S. Soundarya, N. M. Kumar, Green synthesis, characterization and biological activities of nanoceria, Ceram. Int. 45 (2019) 12382–12386, https://doi.org/10.1016/J.CERAMINT.2019.03.164.
[28] A.M. Flank, C.P.C. Aix-marseille, I.F.R. Pole, Cytotoxicity of CeO 2 Nanoparticles Physico-Chemical Insight of the Cytotoxicity Mechanism, Environ. Sci. Technol. 6151–6156 (2006).
[29] L.P. Babenko, N.M. Zholobak, A.B. Shcherbakov, S.I. Voychuk, L.M. Lazarenko, M. Y. Spivak, Antibacterial activity of cerium colloids against opportunistic microorganisms in vitro, Mikrobiol. z. 74 (2012) 54–62.
[30] M.A. Davoodbasha, K. Saravanakumar, A.M. Abdulkader, S.Y. Lee, J.W. Kim, Synthesis of Biocompatible Cellulose-Coated Nanoceria with pH-Dependent Antioxidant Property, ACS Appl. Bio Mater. 2 (2019) 1792–1801, https://doi.org/10.1021/ACSABM.8B00647/SUPPL_FILE/MT8B00647_SI_002.PDF.
[31] J.D. Weaver, C.L. Stabler, Antioxidant cerium oxide nanoparticle hydrogels for cellular encapsulation, Acta Biomater. 16 (2015) 136–144, https://doi.org/10.1016/J.ACTBIO.2015.01.017.
[32] D. Bhattacharya, R. Tiwari, T. Bhatia, M.P. Purohit, A. Pal, P. Jagdale, M.K. R. Mudiam, B.P. Chaudhari, Y. Shukla, K.M. Ansari, A. Kumar, P. Kumar, V. Srivastava, K.C. Gupta, Accelerated and scarless wound repair by a multicomponent hydrogel through simultaneous activation of multiple pathways, Drug Deliv, Transl. Res. 9 (2019) 1143–1158, https://doi.org/10.1007/S13346-019-00660-Z/FIGURES/7.
[33] R. Cuahtecontzi-Delint, M.A. Mendez-Rojas, E.R. Bandala, M.A. Quiroz, S. Recillas, J.L. Sanchez-Salas, Enhanced antibacterial activity of CeO2 nanoparticles by surfactants, Int. J. Chem. React. Eng. 11 (2013) 781–785, https://doi.org/10.1515/IJCRE-2012-0055/MACHINEREADABLECITATION/RIS.
[34] M. Salvador, G. Gutiérrez, S. Noriega, A. Moyano, M. Carmen Blanco-López, M. Matos, Molecular Sciences Microemulsion Synthesis of Superparamagnetic Nanoparticles for Bioapplications, (2021). Doi: 10.3390/ijms22010427.
[35] S. Bazsefidpar, A. Moyano, G. Gutiérrez, M. Matos, M.C. Blanco-López, Lipid–Polymer Hybrids Encapsulating Iron-Oxide Nanoparticles as a Label for Lateral Flow Immunoassays, Biosens. 2021, Vol. 11, Page 218. 11 (2021) 218. Doi: 10.3390/BIOS11070218.
[36] J.D. Hoyos-Leyva, L.A. Bello-Pérez, J. Alvarez-Ramirez, H.S. Garcia, Microencapsulation using starch as wall material: A review, Doi: 10.1080/87559129.2016.1261298. 34 (2017) 148–161. Doi: 10.1080/87559129.2016.1261298.
[37] N. Subpuch, T.-C. Huang, P. Suwannaporn, Enzymatic Digestible Starch from Pyrodextrinization to Control the Release of Tocopheryl Acetate Microencapsulation in Simulated Gut Model (2014), https://doi.org/10.1016/j.foodhyd.2014.10.012.
[38] J. No, M. Shin, Preparation and characteristics of octenyl succinic anhydride-modified partial waxy rice starches and encapsulated paprika pigment powder, Food Chem. 295 (2019) 466–474, https://doi.org/10.1016/J.FOODCHEM.2019.05.064.
[39] V. Marchianò, M. Matos, M. López, S. Weng, E. Serrano-Pertierra, S. Luque, M. C. Blanco-López, G. Gutiérrez, Nanovesicles as Vanillin Carriers for Antimicrobial Applications, Membranes (basel). 13 (2023) 95, https://doi.org/10.3390/MEMBRANES13010095/S1.
[40] M. Romeo, K. Bak, J. El Fallah, F. Le Normand, L. Hilaire, XPS Study of the reduction of cerium dioxide, Surf. Interface Anal. 20 (1993) 508–512, https://doi.org/10.1002/sia.740200604.
[41] F. Le Normand, J. El Fallah, L. Hilaire, P. Légaré, A. Kotani, J.C. Parlebas, Photoemission on 3d core levels of Cerium: An experimental and theoretical investigation of the reduction of cerium dioxide, Solid State Commun. 71 (1989) 885–889, https://doi.org/10.1016/0038-1098(89)90555-3.
[42] J. El Fallah, L. Hilaire, M. Roméo, F. Le Normand, Effect of surface treatments, photon and electron impacts on the ceria 3d core level, J. Electron Spectros. Relat. Phenomena. 73 (1995) 89–103, https://doi.org/10.1016/0368-2048(94)02266-6.
[43] J.Z. Shyu, W.H. Weber, H.S. Gandhi, Surface characterization of alumina-supported ceria, J. Phys. Chem. 92 (1988) 4964–4970, https://doi.org/10.1021/j100328a029.
[44] J.F. Moulder, W.F. Stickle, P.E. Sobol, K.D. Bomben, Handbook of X-ray Photoelectron Spectroscopy, Physical Electronics Inc., Eden Prairie, Minnesota, 1992.
[45] I. Albuquerque, P. Farias, C.C. Lima, F. Santos, S. Correia, Antimicrobial Activity of Cerium Oxide Nanoparticles on Opportunistic Microorganisms: A Systematic Review (2018), https://doi.org/10.1155/2018/1923606.
[46] C. Takahashi, S. Saito, A. Suda, N. Ogawa, Y. Kawashima, H. Yamamoto, Antibacterial activities of polymeric poly(DL-lactide-co-glycolide) nanoparticles and Soluplus® micelles against Staphylococcus epidermidis biofilm and their characterization, RSC Adv. 5 (2015) 71709–71717, https://doi.org/10.1039/C5RA13885J.
[47] B. Bonev, J. Hooper, J. Parisot, Principles of assessing bacterial susceptibility to antibiotics using the agar diffusion method, (n.d.). Doi: 10.1093/jac/dkn090.
[48] M.B. Vásconez, S.K. Flores, C.A. Campos, J. Alvarado, L.N. Gerschenson, Antimicrobial activity and physical properties of chitosan–tapioca starch based edible films and coatings, Food Res. Int. 42 (2009) 762–769, https://doi.org/10.1016/J.FOODRES.2009.02.026.